Earth Surface Processes and Landforms
Earth Surf. Process. Landforms **28**, 689–705 (2003)
Published online in Wiley InterScience (www.interscience.wiley.com). DOI: 10.1002/esp.466

FLOW REVERSAL OVER A NATURAL POOL–RIFFLE SEQUENCE: A COMPUTATIONAL STUDY

ZHIXIAN CAO,[1]*† PAUL CARLING[1] AND ROB OAKEY[2]

[1] *Department of Geography, University of Southampton, Highfield, Southampton SO17 1BJ, UK*
[2] *Department of Geography, University of Lancaster, Lancaster, LA1 4YB, UK*

Received 11 January 2002; Revised 18 July 2002; Accepted 2 October 2002

ABSTRACT

A computational study is presented on the hydraulics of a natural pool–riffle sequence composed of mixed cobbles, pebbles and sand in the River Lune, northern England. A depth-averaged two-dimensional numerical model is employed, calibrated with observed data at the field site. From the computational outputs, the occurrence of longitudinally double peak zones of bed shear stress and velocity is found. In particular, at low discharge there exists a primary peak zone of bed shear stress and velocity at the riffle tail in line with the local maximum energy slope, in addition to a secondary peak at the pool head. As discharge increases, the primary peak at the riffle tail at low flow moves toward the upstream side of the riffle along with the maximum energy slope, showing progressive equalization to the surrounding hydraulic profiles. Concurrently, the secondary peak, due to channel constriction, appears to stand at the pool head, with its value increasing with discharge and approaching or exceeding the primary peak over the riffle. The existence of flow reversal is demonstrated for this specific case, which is attributable to channel constriction at the pool head. A dynamic equilibrium model is presented to reconstruct the pool–riffle morphology. A series of numerical modelling exercises demonstrates that the pool–riffle morphology is more likely produced by shallow flows concentrated with coarse sediments than deep flows laden with low concentrations of fine sediments. It is concluded that channel constriction can, but may not necessarily, lead to competence reversal, depending on channel geometry, flow discharge and sediment properties. Copyright © 2003 John Wiley & Sons, Ltd.

KEY WORDS: pool–riffle; flow reversal; bed shear stress; channel morphology; fluvial processes; mathematical modelling

INTRODUCTION

The hydraulics of flow over pool–riffle sequences in open channels provides a fluid problem of significant interest, as it is critical for understanding sediment transport and morphological evolution processes, and, therefore, it is relevant to river rehabilitation and management. Generally, pools are identified as deep areas with low velocity at low discharges, whereas riffles are areas with steeper water surface slopes and higher velocities at low discharges. Although in natural rivers the cross-section topography can be rather complex, the longitudinal change in bed elevation is the pivotal factor that determines the flow structure. From a fluid dynamics perspective, the role of pool–riffle topography in dictating the flow field is most significant under low-flow conditions, and becomes comparatively less pronounced as discharge increases. The asymptotic state is that the difference in bed elevation over the pool–riffle topography is smaller than flow depth by at least an order of magnitude, and its role in influencing flow structure is essentially negligible.

Most studies on pool–riffle sequences have been built upon the reversal hypothesis due to Keller (1971), such as Lisle (1979), Carling (1991), Keller and Florsheim (1993), Carling and Wood (1994), Miller (1994), Sear (1996), Thompson *et al*. (1998, 1999), Booker *et al*. (2001), to name but a few. Often, reversal refers to the movement of the location of maximum velocity, water surface slope and bed shear stress between pools and riffles under various discharges (Thompson *et al*., 1999). Over the years there has been much debate on the existence of reversal. For instance, according to the three-dimensional (3D) modelling by Booker *et al*. (2001), only three out of a total combination of eight pool–riffle couplets showed reversal in cross-section velocity, and

* Correspondence to: Z. Cao, School of Built Environment, Heriot-watt University, Edinburgh EH14 4AS, UK.
† On leave from Institute of Hydraulic Research, Tianjin University, Tianjin 300072, China.

the difference in velocity between comparable pools and riffles was roughly 10% or less. This undoubtedly makes the existence of reversal on every pool–riffle sequence pairing questionable.

As far as the study methodology for pool–riffle sequences is concerned, field observation is certainly of significance. Unfortunately, this may prove not to be feasible, especially when synchronous measurement of hydraulic elements over the whole flow field, instead of a few points within the flow domain, is to be sought. Computational study is now applicable with the rapid advancement of computer technology. Full 3D modelling has now become realistic (Booker *et al*., 2001), showing great promise for future studies of complicated fluid-flow problems in the water environment compared with previous one-dimensional (1D; Richards, 1978; Carling and Wood, 1994) and two-dimensional (2D; Miller, 1994; Thompson *et al*., 1998) solutions.

This paper aims to study the hydraulics of a natural pool–riffle sequence in the River Lune, northern England, computationally. A depth-averaged 2D model is used, and calibrated using field observation data. The computational outputs are demonstrated to address the flow reversal hypothesis that has been proposed for pool–riffle studies, including velocity and bed shear stress. The implications for sediment transport and maintenance of morphology are addressed with a dynamic equilibrium model.

COMPUTATIONAL MODEL

Basic modelling considerations

Full 3D computational fluid dynamics modelling is certainly the way forward for environmental flows, because it can provide the most detailed information. Over the last two decades it has been extensively used in industrial areas such as aircraft, automotive, heating and ventilation design, as well as in weather forecasting, etc. Yet, in the early stage, its application to natural rivers presents several problems that differ in nature from those in these industrial areas.

Firstly, the free surface of fluvial flows is part of the solution to be acquired. Rigorous treatment of this issue involves the kinematic and dynamic boundary conditions. Current 3D modelling of natural river flows mostly invokes a compromise, i.e. the free surface is computed *a priori* using a separate 1D or depth-averaged 2D hydraulic model, and afterwards the 3D flow field is solved based upon the complete Reynolds-averaged equations implemented with a turbulence closure model. It is noted that the inherent inconsistency and uncertainty of this kind of compromise remain unclear. In fact, the problem of free surface is one of the major issues that need to be addressed properly in future development of 3D models for river flows (Cao and Carling, 2002a,b).

Secondly, difficulty may arise in specifying the bottom boundary conditions due to the heterogeneous composition of bed material and its large size relative to water depth. More specifically, in 3D modelling there is no physically well-grounded approach to establishing the bottom boundary conditions for mean velocity, turbulent energy and dissipation rate, as the bed material protrudes far into the flow (Nezu and Nakagawa, 1993). The riverbed under consideration is composed of a mixture of cobbles, pebbles and sand, and the water flow is shallow, compared with the size of bed material. Typically, the largest cobbles are over 10 cm in size, and can be exposed at the water surface during low discharges.

The difficulties in specifying the bottom boundary conditions and determining the free surface become most acute for low discharge flows, which is plausibly the reason that only intermediate and high flows are simulated by Booker *et al*. (2001). In shallow hydrodynamics it is well known that 2D models can explicitly produce the free surface, and there is no need to specify bottom boundary conditions because the role of the bottom boundary in dictating the flow can be represented in the empirical resistance terms with the use of the Manning roughness parameter. Hence, the difficulty in specifying the free surface and the need to define the bottom boundary conditions for mean velocity and other turbulent quantities, common to 3D models, are obviated. Consequently, a 2D hydraulic model is employed for the present study, which is viewed as a sensible balance between model capability and complexity.

Depth-averaged 2D model

Depth-averaged 2D hydraulic models are built upon the integrated form of the Reynolds-averaged equations derived from mass and momentum conservation laws. Here, a simple turbulent closure model is introduced

based on the Boussinesq eddy viscosity concept. Presently, 2D models are widely used in aquatic environment modelling practice, thus only a brief description is given below.

The governing equations read

$$\frac{\partial h}{\partial t} + \frac{\partial (hu)}{\partial x} + \frac{\partial (hv)}{\partial y} = 0 \tag{1}$$

$$\frac{\partial u}{\partial t} + u\frac{\partial u}{\partial x} + v\frac{\partial u}{\partial y} + g\frac{\partial (h+z)}{\partial x} = -f_x + \frac{1}{h}\frac{\partial (h\sigma_{xx})}{\partial x} + \frac{1}{h}\frac{\partial (h\sigma_{xy})}{\partial y} \tag{2}$$

$$\frac{\partial v}{\partial t} + u\frac{\partial v}{\partial x} + v\frac{\partial v}{\partial y} + g\frac{\partial (h+z)}{\partial y} = -f_y + \frac{1}{h}\frac{\partial (h\sigma_{yx})}{\partial x} + \frac{1}{h}\frac{\partial (h\sigma_{yy})}{\partial y} \tag{3}$$

where t, x, y are time, longitudinal and transverse coordinates respectively, u and v are the depth-averaged mean velocities in x and y respectively, h is the local flow depth, g is the gravitational acceleration, z is the bed elevation relative to datum, f_x and f_y are the resistance components due to bottom friction in x and y respectively, and σ_{xx}, σ_{xy}, σ_{yx} and σ_{yy} are the depth-averaged Reynolds stresses. The following are introduced to close the bed resistance and Reynolds stresses:

$$f_x = \frac{gn^2 u\sqrt{u^2+v^2}}{h^{4/3}}, \quad f_y = \frac{gn^2 v\sqrt{u^2+v^2}}{h^{4/3}} \tag{4}$$

$$\sigma_{xx} = 2\nu_t\frac{\partial u}{\partial x}, \quad \sigma_{yy} = 2\nu_t\frac{\partial v}{\partial y}, \quad \sigma_{xy} = \sigma_{yx} = \nu_t\left(\frac{\partial v}{\partial x} + \frac{\partial u}{\partial x}\right) \tag{5}$$

where n is the Manning roughness parameter and ν_t is the turbulent eddy viscosity. For simplicity, a zero-equation turbulence closure model is used, rendering

$$\nu_t = \lambda u_* h \tag{6}$$

where u_* is the bed shear velocity and λ is a coefficient. For idealized steady and uniform flows, $\lambda = \kappa/6$ ($\kappa = 0{\cdot}4$; von Karman constant). For natural river flows, there exists an additional mechanism that needs to be considered in depth-averaged models, i.e. dispersion resulting from non-uniform profiles of mean velocity components (Nezu and Nakagawa, 1993). Mathematically, the dispersion can be incorporated into the turbulent stress terms in Equations (2) and (3) by tuning the coefficient λ in Equation (6). In fact, this is similar to the so-called non-dimensional 'eddy viscosity' in the lateral momentum model for compound channel flows developed by Shiono and Knight (1991), which is reported to range between 0·07 and 0·5. In the present computation, $\lambda = 0{\cdot}1$ is used.

For easy specification of boundary conditions, the upstream and downstream boundaries are defined within reaches of comparatively regular plan geometry (e.g. banks roughly paralleling the longitudinal coordinate) so that the transverse velocity can be neglected ($v \approx 0$). At both the upstream and downstream boundaries, the flow depths are determined according to given water stages, and the longitudinal velocity u is computed using the model of Shiono and Knight (1991). For simplicity, the side-wall (riverbank) boundary conditions are approximately specified so that the mean velocity vanishes (i.e. no-slip velocity condition).

To expedite the numerical solution, the irregular physical flow domain in (x, y) is transformed to a square computational domain in (ζ, η) $\in$ [0, 1] by a simple geometrical transformation. Referring to Figure 1, this can be expressed as

$$\begin{cases} \zeta = x/L \\ \eta = (y - y_1)/(y_2 - y_1) \end{cases} \tag{7}$$

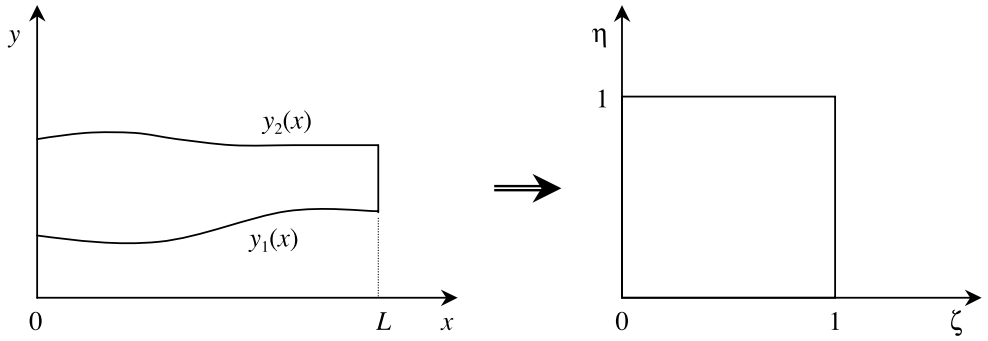

Figure 1. Physical and computational domains

where L is the length of the study reach in x, and y_1 and y_2 are functions of x featuring the left and right riverbanks respectively. The resulting equations in the computational domain are numerically solved for mean velocity components and depth using the MacCormack scheme, which is explicit and second-order accurate in both time and space. The diffusion terms are discretized following Yulistiyanto *et al*. (1998). For steady flow modelling, the time-marching method is employed to achieve convergence solutions. The convergence criterion is defined as the relative error tolerance $\varepsilon \equiv abs(\varphi^{k+1} - \varphi^k)/abs(\varphi^k) \leq 0{\cdot}001$, where $\varphi \equiv [h, u, v]$, and the superscript k denotes time step. The computation is carried out with a mesh of 150×15, after a number of numerical experiments with differing meshes that demonstrate mesh-independent outputs.

MODEL CALIBRATION USING FIELD DATA

Field observations were carried out at the field site, the River Lune in northern England, of which the details are described in Oakey (2002). At the low and essentially steady flow, the free surface elevation along the study reach was measured. Also, during a 6 day flood event (25 February to 2 March 2001), the water stage was synchronously measured at the up- and down-stream cross-sections as well as at an additional cross-section roughly at the middle of the study reach. These data are employed to calibrate the 2D model described above. The Manning roughness parameter is tuned so that the computed free surface profiles match the observations.

Table I summarizes the hydraulic information for three distinct flow cases, i.e. low, medium and high flows. For the low and essentially steady flow, modelling tests show that: (a) it is necessary to use distributed roughness in order to match the measured free surface; (b) the roughness is strongly dependent upon the local depth. Physically, this is attributable to the nature of shallow flow in comparison with the large bed material size, especially over the riffle, as stated earlier. Some evidence of support for the dependence of roughness on local depth is provided by the experimental study of Barros and Colello (2001) on surface roughness for shallow overland flow. To a certain extent, the flow over the riffle in the low-flow case is similar to overland flow, as the largest cobbles protrude through the free surface. The medium flow case in Table I is designed as the 'peak flow' roughly during the 6 day flood event (25 February to 2 March 2001). Strictly speaking, the medium flow was unsteady if considered within the time scale of the full flood event. However, the medium flow status lasted over half an hour without appreciable change in water stages, which is by far greater than the time $T = L/min[abs(U \pm \sqrt{gR})] < 180{\cdot}0$ seconds, required for flow disturbances to propagate through the entire study channel. Hence, it is reasonable to view the medium flow as approximately quasi-steady in the modelling. In the above, L, U and R are respectively the channel length, the cross-section-averaged velocity, and the hydraulic radius. Calibration shows that a fixed value of 0·04 of the roughness parameter can give satisfactory agreement with the measured water stage. The high flow in Table I corresponds to the 'peak flow' during the flood process from 8 to 16 December 2000. For the high flow the roughness is set to be equal to 0·04, as for the medium flow case, by referring to the reasoning that the roughness parameter should be less sensitive to bed material size as the relative depth increases. For all the three flow cases, the free surface is shown in Figure 2 along with the bed elevation.

Table I. Hydraulic parameters for low-, medium- and high-flow cases

Flow case	Water stage (m)		Discharge ($m^3 s^{-1}$)	Manning roughness n
	Inlet	Outlet		
Low	–2·90	–3·70	1·02	$\max[0{\cdot}04,\ 0{\cdot}04 + 6.0(0{\cdot}4 - h)^3]$
Medium	–2·51	–3·19	6·17	0·04
High	–2·03	–2·74	16·83	0·04

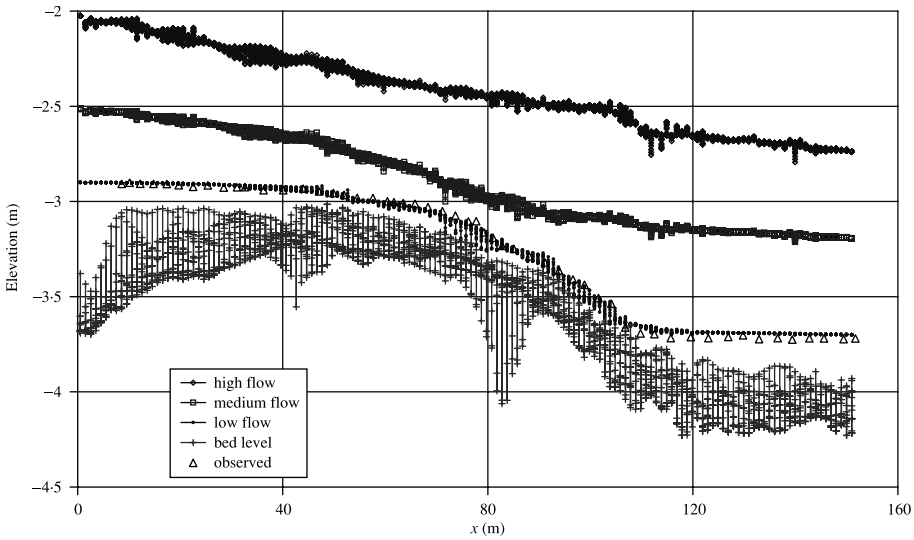

Figure 2. Free surface and bed elevation for a natural pool–riffle sequence in the River Lune

BED SHEAR STRESS AND VELOCITY DISTRIBUTION PATTERNS

Figure 3 shows the bed shear stress distributions in relation to the low, medium and high flows as summarized in Table I, along with the channel bed topography. These are also illustrated in Figure 4 for a clear picture of the longitudinal variations with the bed elevation. Apparently, under the low-flow case in Figures 3 and 4, a primary peak zone of bed shear stress occurs around the riffle tail at $x \in [90\ \text{m}, 105\ \text{m}]$, with its value being up to about 80 N m^{-2}. At the same time there exists a secondary peak within $x \in [105\ \text{m}, 120\ \text{m}]$ at the pool head, of which the peak value (20 N m^{-2}) is significantly smaller than the primary peak. As discharge increases in the medium and high flows, the existence of double peak zones of bed shear stress becomes more clearly distinguishable. In particular, the peak zone at the riffle tail under the low-flow case tends to move progressively toward the upstream side of the riffle, and there seems to be longitudinal equalization of bed shear stress over the riffle. Quantitatively, the value of this peak bed shear stress reads 60 N m^{-2} and 56 N m^{-2}, located around $x \in [70\ \text{m}, 80\ \text{m}]$ and $x \in [30\ \text{m}, 36\ \text{m}]$ respectively, in the medium and high flow cases (Figure 4), whilst the bed shear stress at the riffle tail increases with discharge. Concurrently, the other peak zone of bed shear stress appears to remain at the pool head $x \in [105\ \text{m}, 120\ \text{m}]$ irrespective of discharge, and its value increases with discharge (24 N m^{-2} and 56 N m^{-2} respectively at medium and high flows).

The computed depth-averaged velocity is shown in Figures 5 and 6. In line with the nature of distribution of bed shear stress described above, the velocity distribution exhibits a rather complex pattern. Under the low-flow case, the transverse fluid motion is strongly developed compared with its streamwise counterpart. More specifically, the flow path clearly follows the locally lowest bed topography, with the velocity almost vanishing in, for instance, the upper (near left-bank) area for $x \in [42\ \text{m}, 60\ \text{m}]$ due to small flow depth there, as shown in

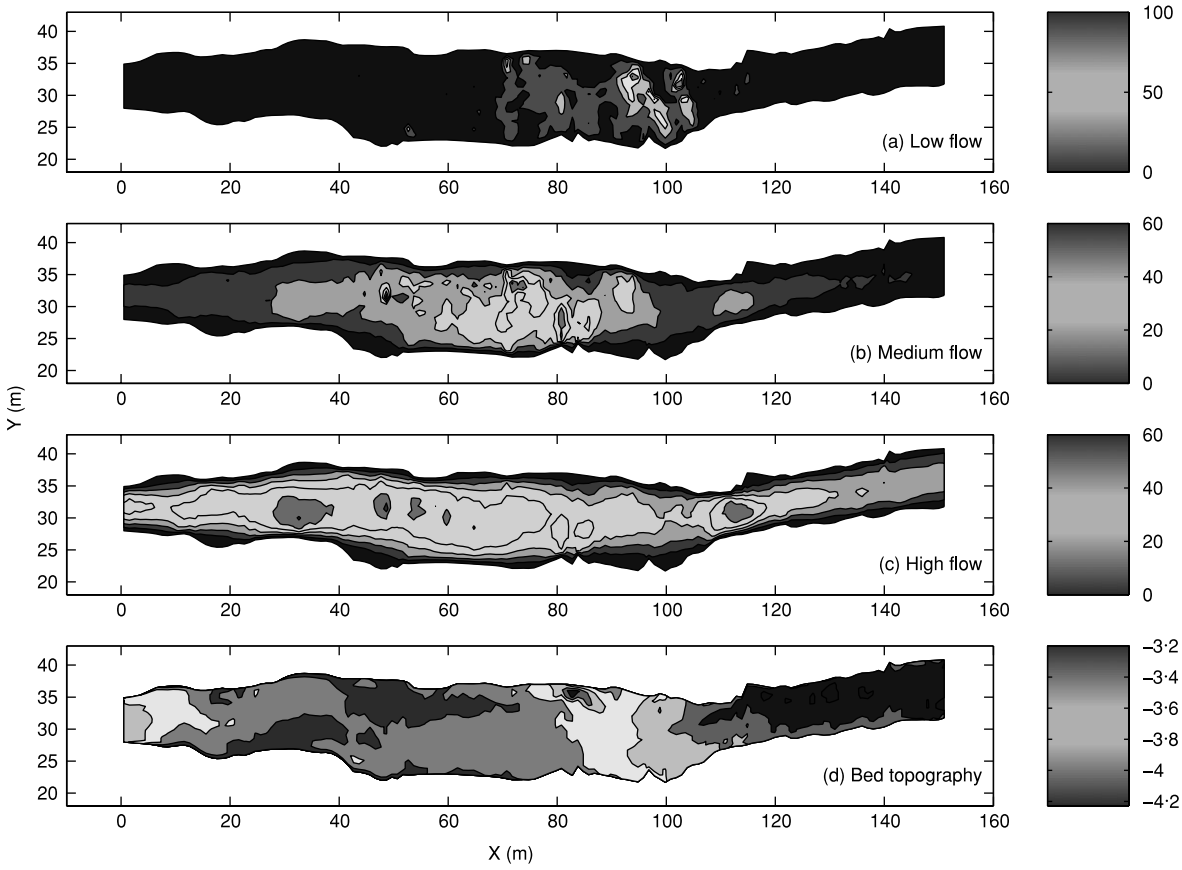

Figure 3. Contour of bed shear stress (N m^{-2}) at (a) low, (b) medium and (c) high flows; (d) riverbed topography (m). Flow from left to right

Figures 5(a) and 3(d). This feature of the low-flow case contrasts with the medium and high flows, in which the longitudinal motion dominates (Figure 5). Quantitatively, the transverse velocity ranges between −0·4 and +0·4 m s^{-1} for all the low, medium and high flows, whereas the streamwise velocity increases greatly with discharge (Figures 5 and 6).

Physically, the pattern of velocity is mainly determined by the relative dominance of gravitational action under low flow and its transition to that of an inertia effect in medium and high flows. To clarify, the Froude number defined using the streamwise velocity, $Fr = u/\sqrt{gh}$, is shown in Figure 7. The Froude number increases with discharge, indicating the transition of gravitational dominance in low flow to that of inertia under medium and high flows. It is also interesting to note that the pattern of spatial distributions of Froude number is similar to that of bed shear stress, including the occurrence of double peak zones longitudinally; see Figures 4 and 7. It follows that the complex pattern of bed shear stress is essentially dictated by the relative importance of gravitational action and inertia.

As the gravitational action prevails, the bed topography plays a leading role as at the low flow. This explains why the peak bed shear stress and velocity occur at the riffle tail (Figures 4 and 6) at $x \in$ [90 m, 105 m], where the energy slope reaches a maximum (Figure 2). When inertia predominates at higher discharges, the effect of the pool–riffle bed topography decreases gradually. That is why there is an evident equalization in both bed shear stress and velocity over the riffle area (Figures 4 and 6), except at the pool head.

The patterns of bed shear stress and velocity are also affected by channel plan geometry, in addition to bed topography. Most notably, the channel constricts to roughly 7 m in width at about $x = 108$ m. It is this constriction that results in the occurrence of the standing peak zone of bed shear stress and velocity at the pool head,

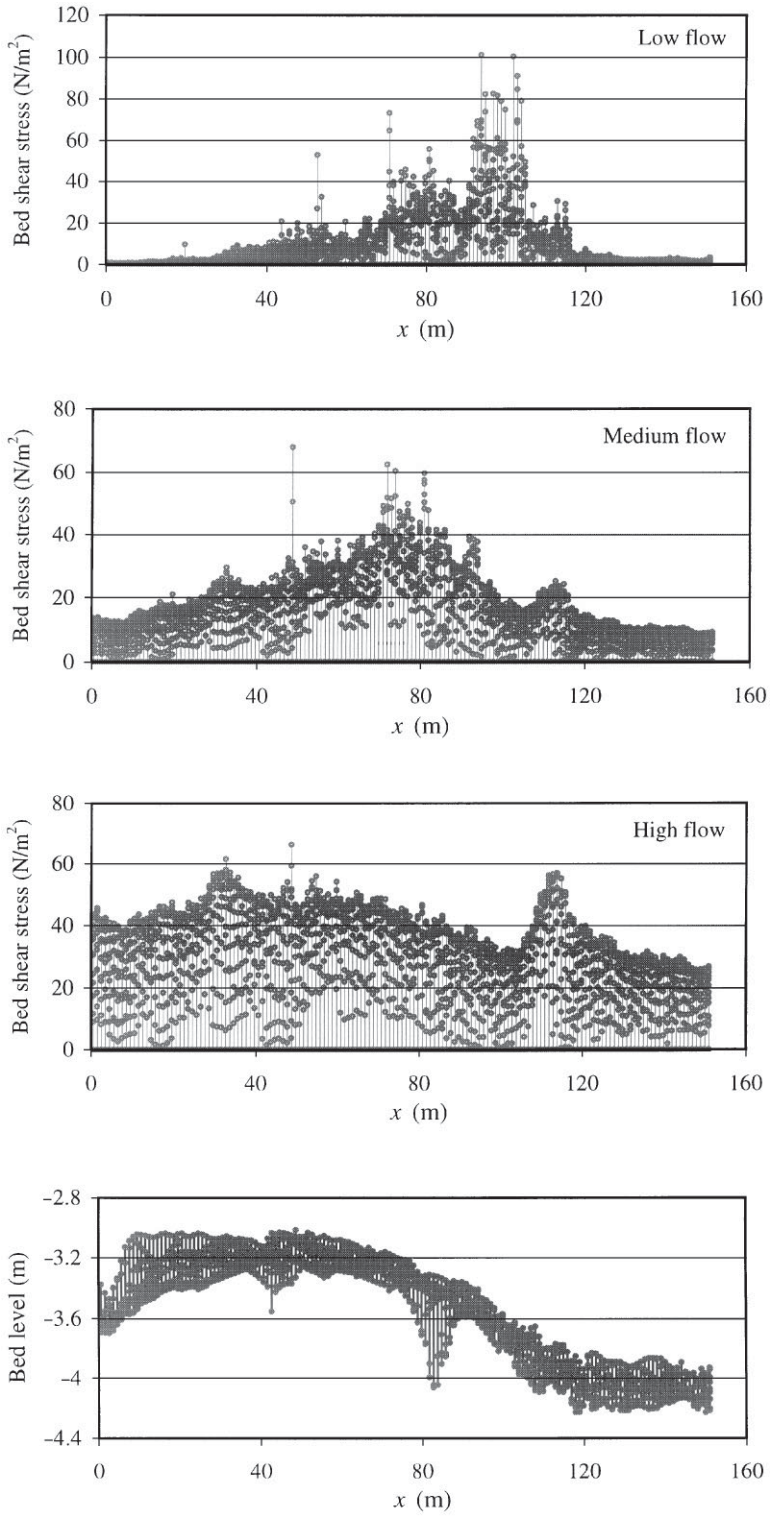

Figure 4. Bed shear stress distributions at low, medium and high flows and riverbed elevation

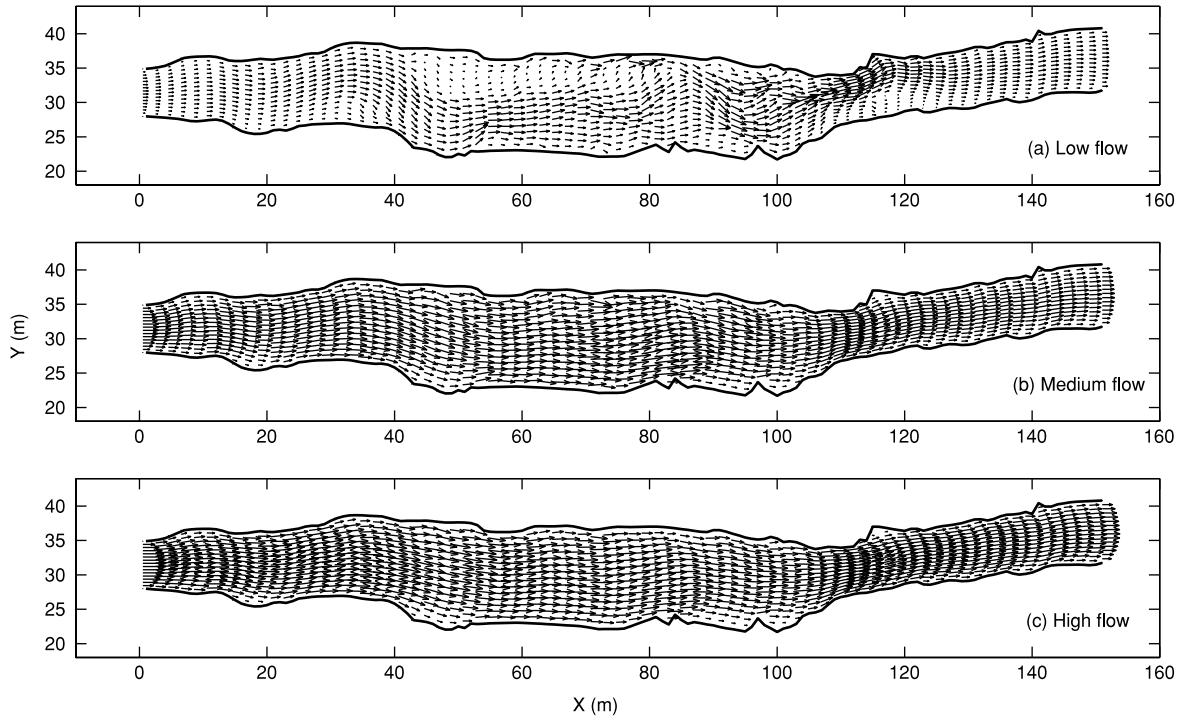

Figure 5. Computed velocity fields at low, medium and high flows (velocity scale: 1 cm equivalent to 3·6 m s^{-1})

which is more appreciable in the medium and high flows (Figures 4 and 6). Channel constriction has, for a long time, been known to lead to increased bed shear stress and, subsequently, to local scour of the bed (Lim, 1993; Lim and Cheng, 1998). Thompson *et al*. (1998, 1999) considered the role of vanes in regulating the flow over a pool–riffle sequence, which is a very special case in natural rivers. Further discussions in this vein will be provided in the next section with respect to flow reversal and pool–riffle morphology.

OCCURRENCE OF FLOW REVERSAL

The occurrence of the longitudinally double peak zones of bed shear stress, velocity and Froude number and its distinct feature in relation to differing discharges are the product of both the pool–riffle bed topography and plan geometry (Figures 3–7). It is the longitudinal profile of bed elevation that results in the primary peak zone of bed shear stress, velocity and Froude number over the riffle. The location of its occurrence in response to different discharges is determined by the relative importance of gravitational and inertia effects. It is a theoretically self-evident fact that there must be equalization of bed shear stress and velocity in line with increasing discharge because the longitudinal change of bed elevation tends to have less effect under deep flows. The ultimate limiting state is that the discrepancy between bed elevations at the pool centre and riffle crest is negligible compared with flow depth, and the flow is approximately longitudinally uniform, which implies the disappearance of the primary peak zone over the riffle.

For flow reversal to take place there must be a separate mechanism that is competent enough to change the flow at the pool so that a secondary peak zone occurs and exceeds the primary peak over the riffle. One cannot expect this from the longitudinal variation in bed elevation. Carling and Wood (1994) found that a hydraulically rougher pool in comparison with the riffle could promote the occurrence of reversal. Alternatively, a channel constriction at the pool head can have a similar effect, which is the case for the pool–riffle sequence in the River Lune in the present study (Figures 3–7). From a 1D hydraulics point of view, channel constrictions can cause increased resistance. In this vein, the role of constriction in dictating the occurrence of the secondary peak zone

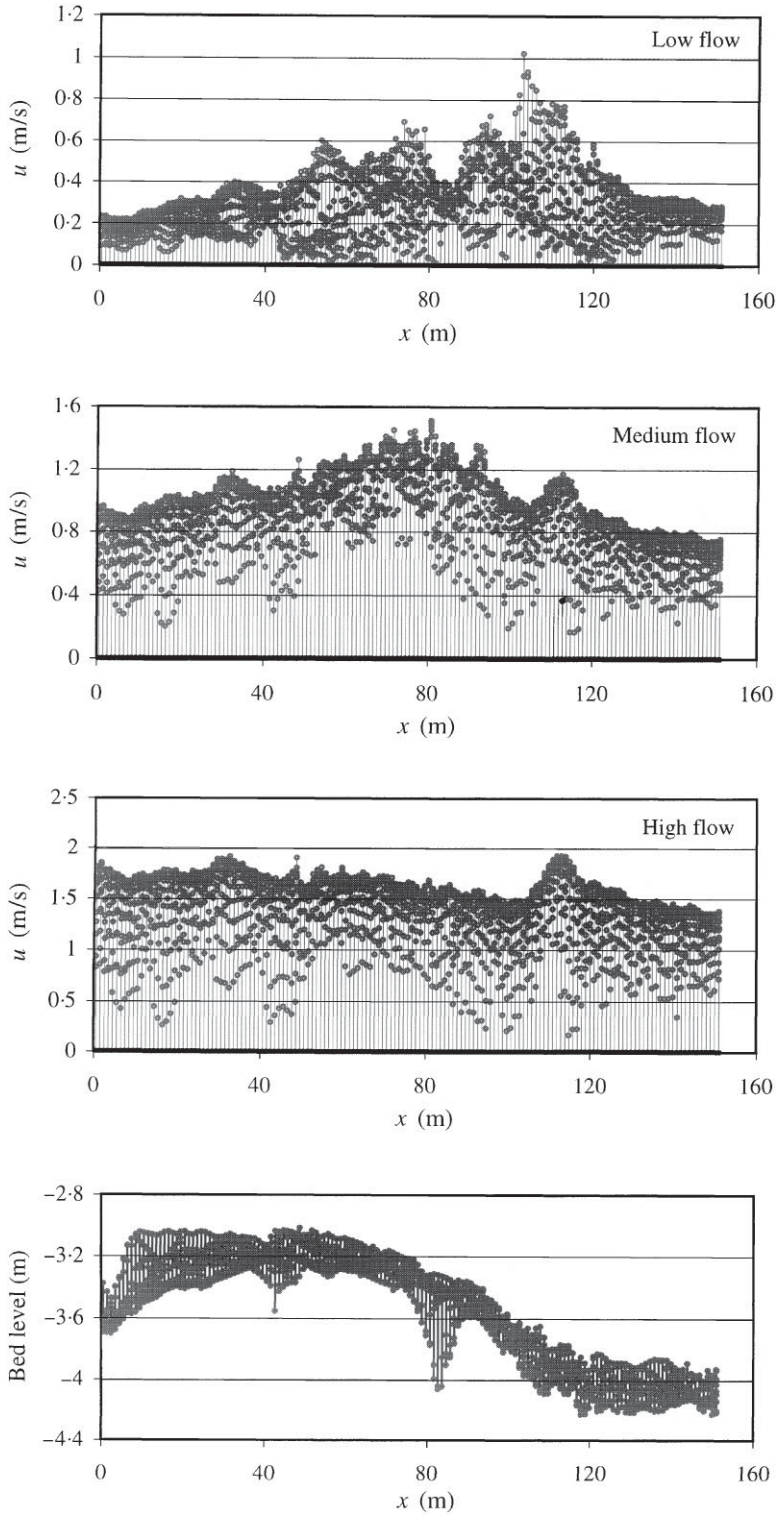

Figure 6. Streamwise velocity at low, medium and high flows

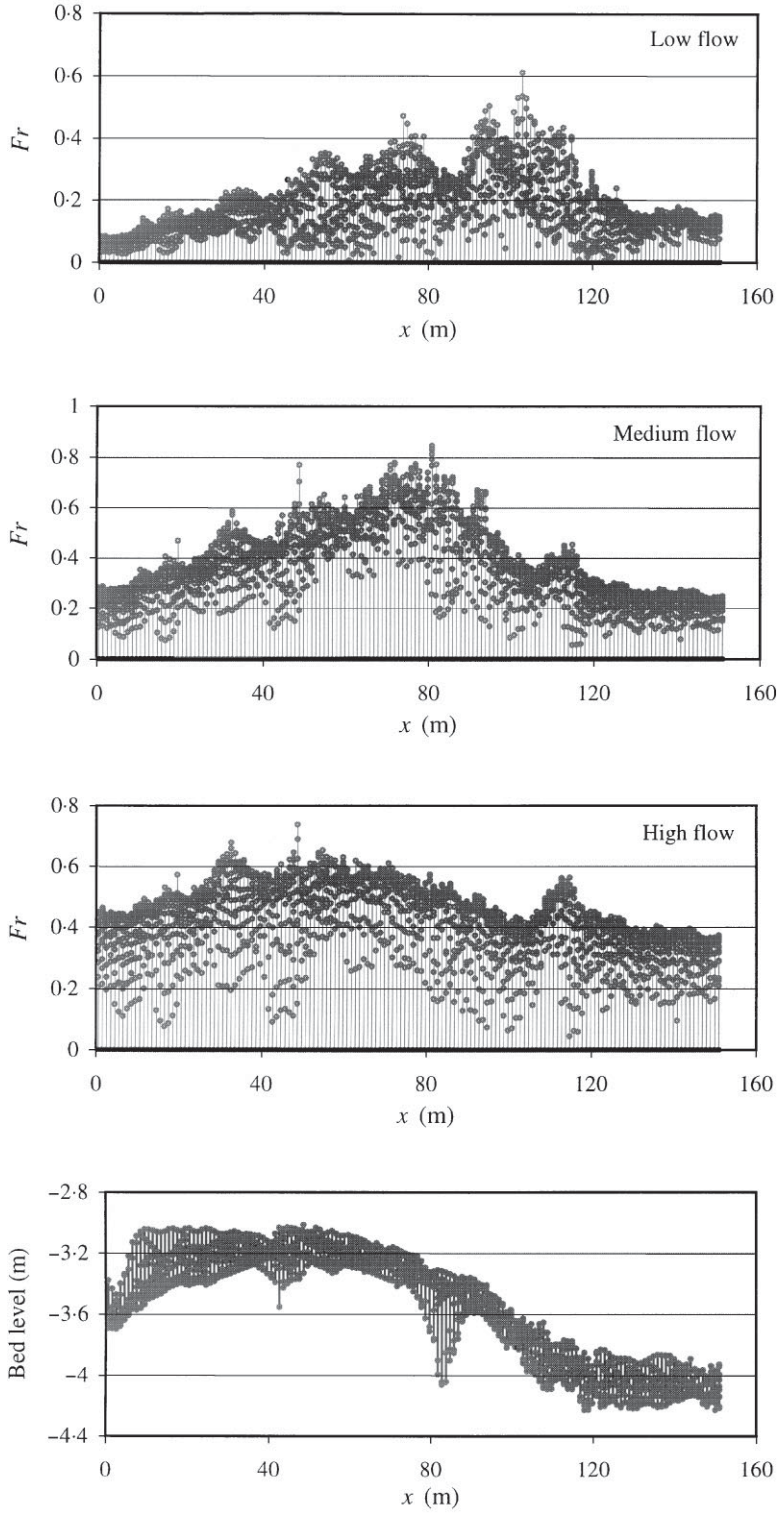

Figure 7. Froude number at low, medium and high flows

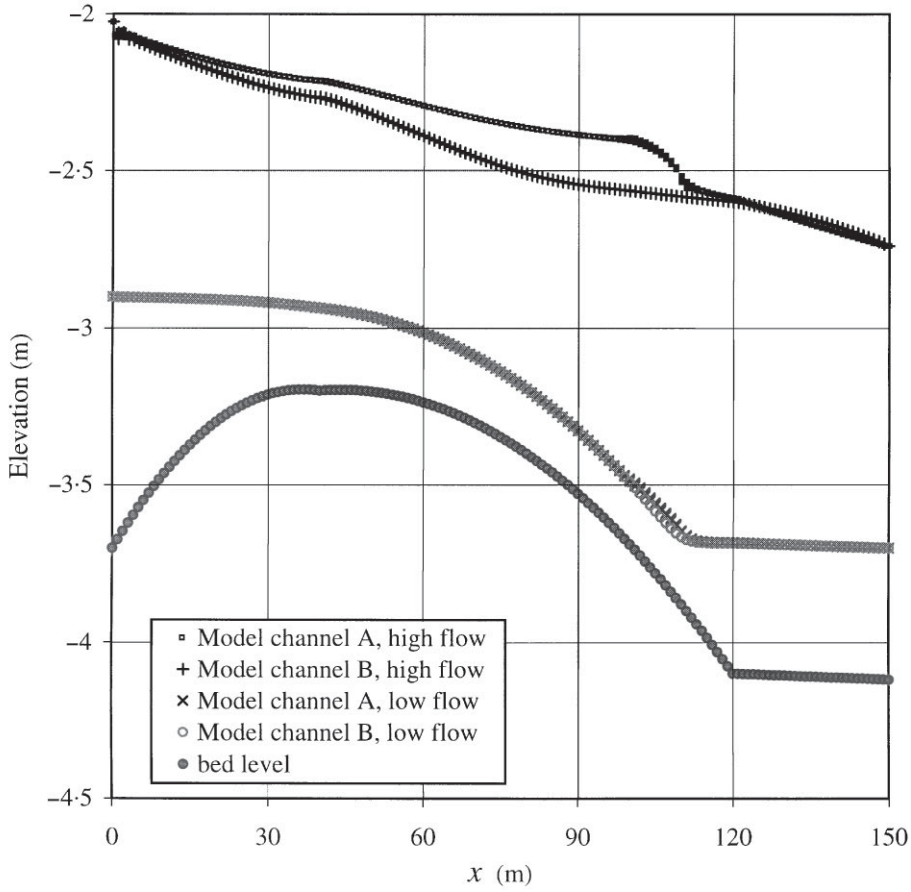

Figure 8. Free surface and bed elevation for pool–riffle sequence, model channels A and B

at the pool head (and subsequently reversal) is equivalent to that of a hydraulically rougher pool presumed in the modelling exercise by Carling and Wood (1994), although large roughness can be induced by factors other than constriction.

To ascertain further the role of channel constriction and complement the modelling exercise by Carling and Wood (1994), two model channels were constructed and the corresponding flows simulated in relation to the up- and down-stream water stages and roughness in the low- and high-flow cases as listed in Table I. The computational free surface and bed shear stress are shown in Figures 8–10. The plan geometry and bed topography of model channel A are approximately abstracted from the study reach in the River Lune (Figures 3d and 2), with the transverse variation in bed elevation being neglected (Figure 8) and the channel banks being straightened (Figure 9a and b). The model channel B is similar to model channel A, except that there is no constriction in channel width at $x = 110$ m (Figure 9c and d). Apparently, there is no flow reversal at the high-flow case for model channel B without a constriction, whereas the occurrence of reversal in model channel A is evident. The pattern of velocity is qualitatively similar to that of bed shear stress in Figure 10, and thus is not shown here. It is noted that the disparity between the flows in model channels A and B, under the low-flow case, is only marginal. However, in the high flow the disparity is significant not only in free surface (Figure 8), but also in bed shear stress (Figures 9 and 10). Therefore, it is implied that channel constriction has a greater impact on the flow at high discharges than at low discharges.

A previous observation that flow reversal is mostly seen at high discharges (Carling and Wood, 1994) appears to support the present finding on the occurrence of flow reversal. As demonstrated in Figures 3, 4, 6, 9, and 10, at higher discharges, the primary peak zone of bed shear stress and velocity over the riffle diminishes (echoing

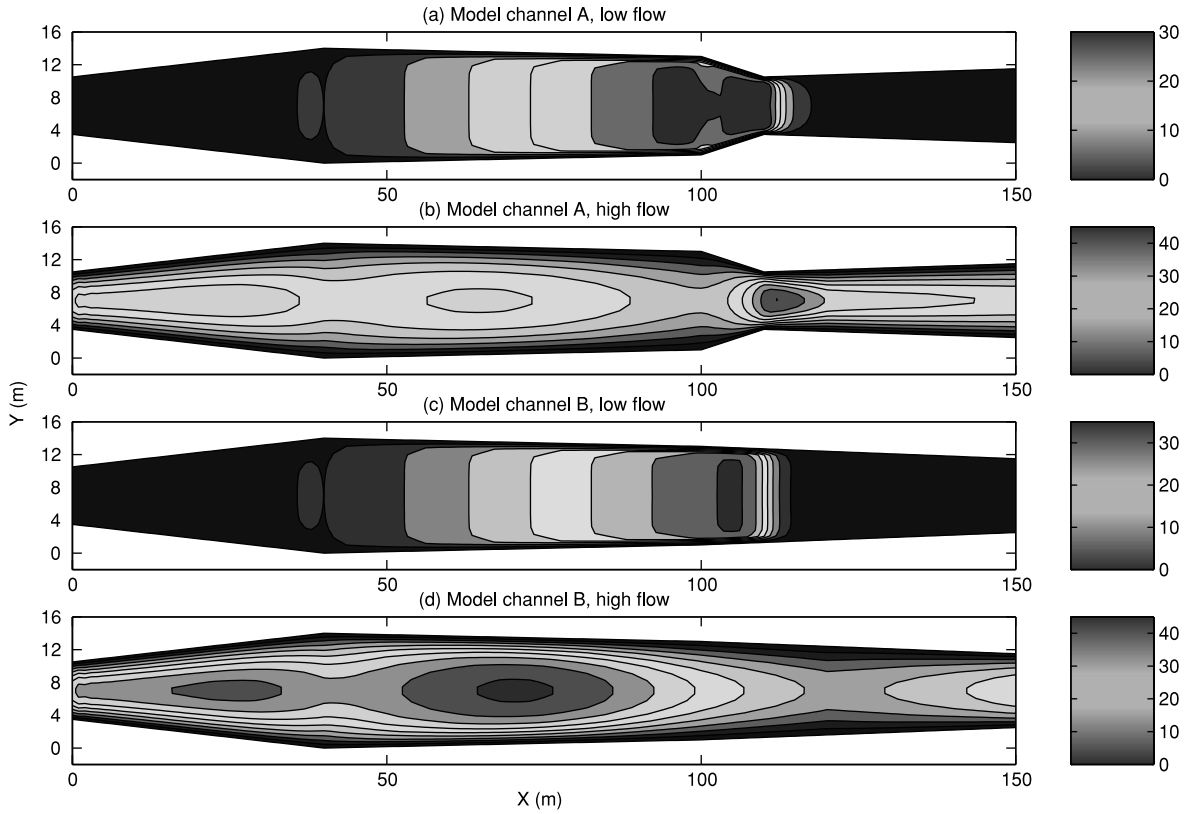

Figure 9. Contour of bed shear stress (N m^{-2}) at low- and high-flow cases, model channels A and B. Flow from left to right

the equalization), while the secondary peak zone standing at the pool head evolves. Hence, it is natural for bed shear stress and velocity at the pool head to approach or even exceed those over the riffle at high discharges.

POOL–RIFFLE MORPHOLOGY: A DYNAMIC EQUILIBRIUM MODEL

Any stable bed morphology in alluvial rivers can be viewed as an asymptotic state of long-term erosion and deposition. Subject to differing approaching flow and sediment conditions, it can be referred to as a dynamic or a static equilibrium state. If the approaching flow is under threshold for initiation of sediment movement and carries no sediment, then the bed morphology can only be formed by local scour. The corresponding ultimate asymptotic state is normally defined as a static equilibrium state. An example of clear-water scour due to channel contractions can be found in Lim (1993) and Lim and Cheng (1998). Contrarily, it is a dynamic equilibrium state if established by sediment-laden approaching flows.

There appears to have been no attempt to reconstruct the morphology of a pool–riffle sequence, as the current understanding of its formation mechanism remains incomplete. An attempt is made herein to reconstruct the pool–riffle sequence in the River Lune under the present study. We believe that under-threshold clear-water approaching flows may not be competent enough to form such a large-scale morphology in comparison with flow depth and channel dimensions. Thus, it is presumed that the pool–riffle sequence was produced by more energetic sediment-laden approaching flows and represents a dynamic equilibrium state. It is noted that the present pool–riffle sequence in the River Lune may not be in its original dynamic equilibrium state. Instead, it may have evolved further from its initial dynamic equilibrium state under the action of less competent and long-term clear-water moulding. Tracing this post-formation clear-water moulding appears unrealistic, and hence the attempt to reconstruct the pool–riffle sequence can only be qualitative. The following dynamic equilibrium

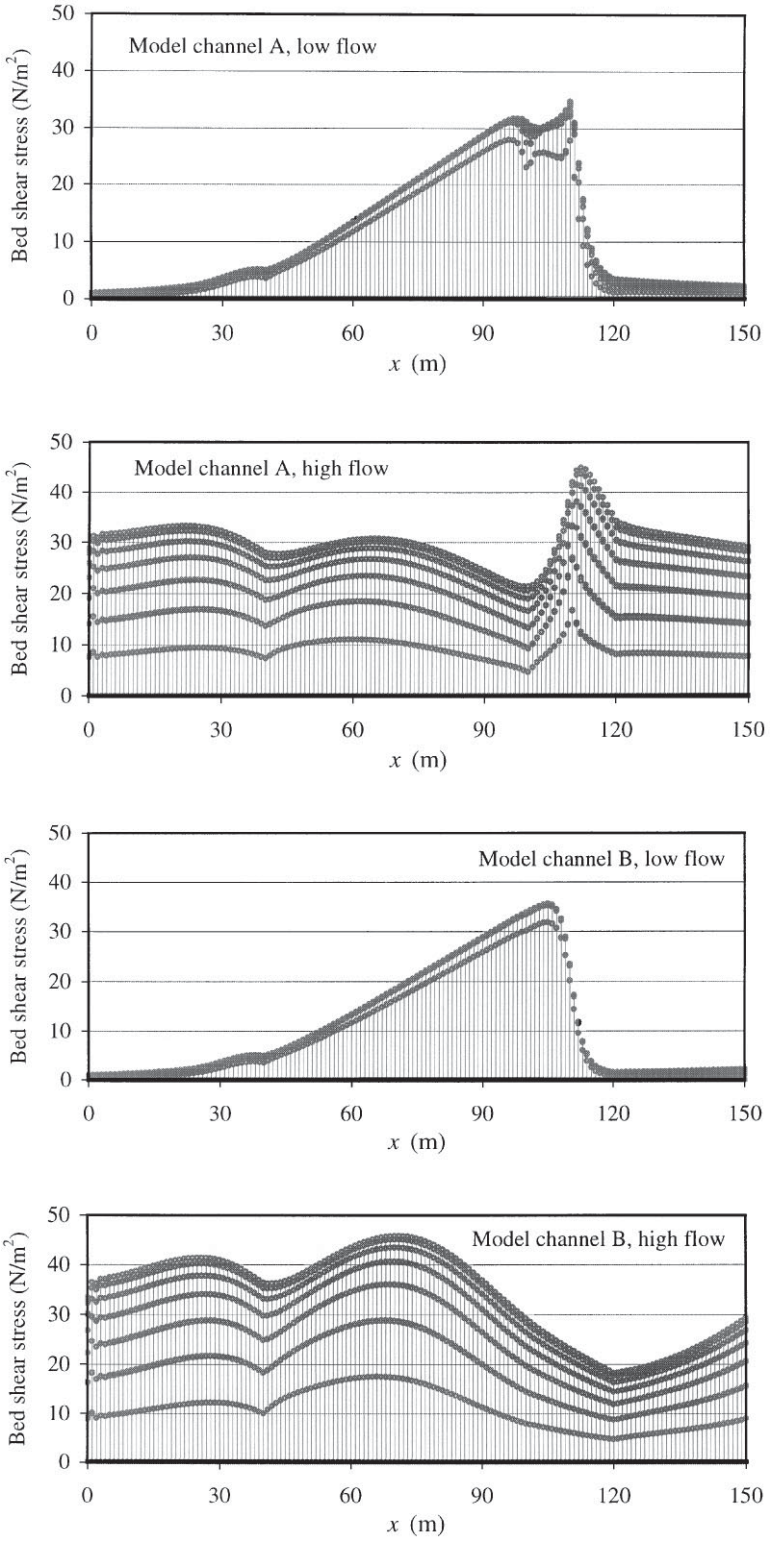

Figure 10. Bed shear stress distributions at low and high flows in model channels A and B

model can be formulated for its reconstruction. For simplicity, the plan configuration of the straightened model channel A (Figure 9a and b) is deployed and a 1D model applied. Also bed-load transport is assumed to dominate. Under the asymptotic equilibrium state, the transient impacts are negligible and the mass conservation equations for the water–sediment mixture and the sediment and the energy conservation for the mixture flow are

$$\frac{\partial(Bhu)}{\partial x} = 0 \tag{8}$$

$$\frac{\partial Q_s}{\partial x} = 0 \tag{9}$$

$$\frac{\partial}{\partial x}\left(z + h + \frac{u^2}{2g}\right) = -S \tag{10}$$

respectively, where B is the channel width, S is the friction slope and Q_s is the sediment transport rate. To close the model, the Manning relationship and the Meyer–Peter and Muller formula for bed-load transport rate are introduced, i.e.

$$S = (nu)^2/h^{4/3} \tag{11}$$

$$Q_s = Bm\sqrt{sgd^3}\,(\theta - \theta_c)^{3/2} \tag{12}$$

where $m = 8{\cdot}0$ is a coefficient, d is the representative diameter of sediment particles, $\theta = \tau_b/\rho gsd$ is the Shields parameter, $\tau_b = \rho ghS$ is the bed shear stress, θ_c is the critical Shields parameter for initiation of sediment movement ($\theta_c \approx 0{\cdot}045$), $s = \rho_s/\rho - 1 = 1{\cdot}65$ is the specific density of sediment, and ρ and ρ_s are the densities of the water and sediment respectively.

Given the approaching flow discharge Q and sediment transport rate Q_s, the flow depth and velocity can be derived from Equations (8) and (9) along with the auxiliary relationships in Equations (11) and (12). Thus

$$u^{7/3} = \frac{sd}{n^2}\left(\frac{Q}{B}\right)^{1/3}\left[\theta_c + \left(\frac{Q_s}{Bm\sqrt{sgd^3}}\right)^{2/3}\right] \tag{13}$$

$$h^{7/3} = \frac{1}{sd}\left(\frac{nQ}{B}\right)^{2}\left[\theta_c + \left(\frac{Q_s}{Bm\sqrt{sgd^3}}\right)^{2/3}\right]^{-1} \tag{14}$$

Integrating Equation (10) between two successive cross-sections i and $i + 1$ leads to Equation (15) for determination of bed elevation, which is second-order accurate (where Δx is the spatial step). The only boundary condition required is the bed or free surface elevation at either the upstream or the downstream end of the computational channel. In the following modelling exercises, the bed elevation ($z = 0$) is arbitrarily specified at the downstream end.

$$z_i = \left(z + h + \frac{u^2}{2g}\right)_{i+1} - \left(h + \frac{u^2}{2g}\right)_i + \frac{\Delta x}{2}(S_i + S_{i+1}) \tag{15}$$

Figure 11 shows the computed bed and free surface elevations (Figure 11a) and also the bed shear stress profiles (Figure 11b) in relation to fixed $Q = 16\ \mathrm{m^3\ s^{-1}}$, $d = 50$ mm, $n = 0{\cdot}04$, but differing sediment transport rates

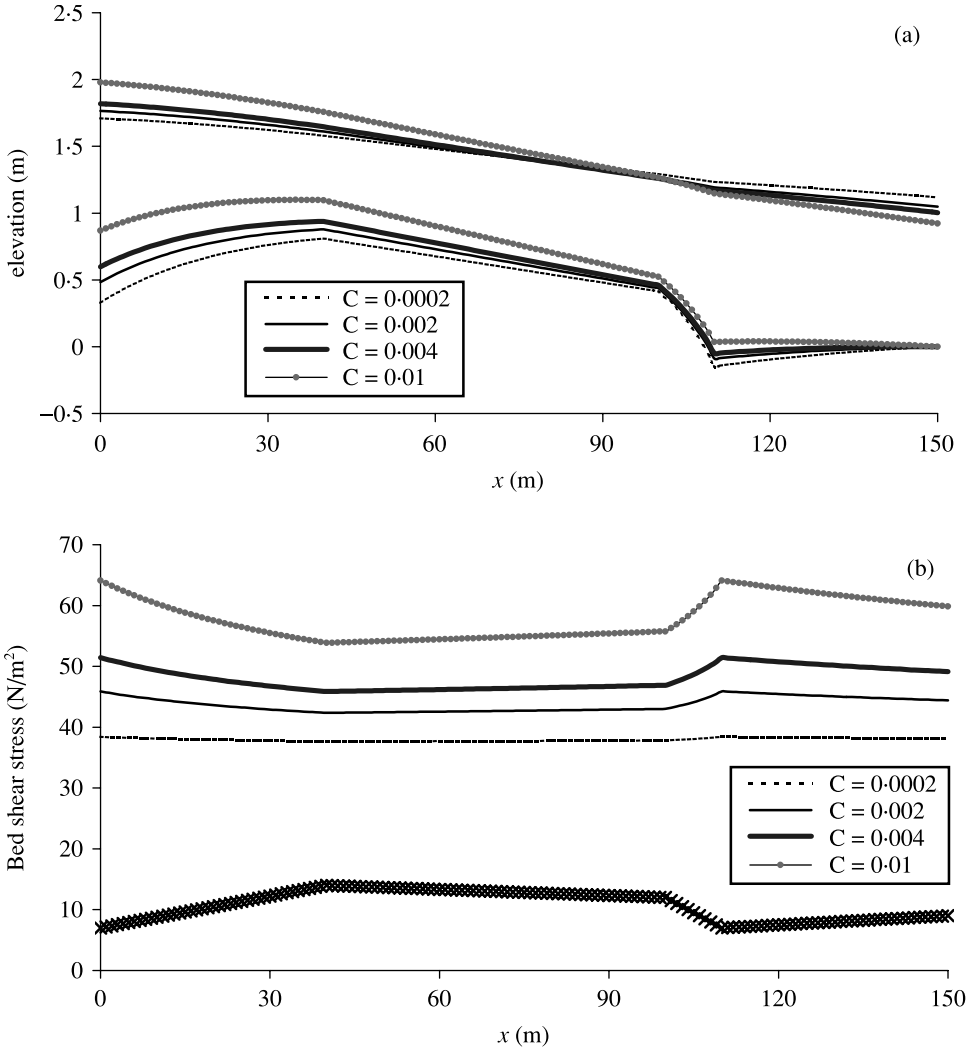

Figure 11. Reconstructed pool–riffle sequences in relation to differing sediment concentrations: (a) bed and free surface profiles; (b) bed shear stress profiles and channel width

($Q_s = QC$; C is the volumetric sediment concentration). The discharge and Manning roughness correspond to those under the high-flow condition listed in Table I, whereas the sediment particle diameter is estimated based on sampled bed material from the River Lune under the present study. The channel width (crosses) is also included in Figure 11b. It is demonstrated in Figure 11a that the pool–riffle morphology can be successfully reconstructed, at least in a qualitative sense, by the present dynamic equilibrium model. The height of the pool–riffle sequence and the average free surface slope increase progressively with sediment transport rate, which can be inferred from the basic sediment transport principle that more competent flow is required to convey more sediments. Concurrently, from Figure 11b the occurrence of reversal in bed shear stress is found in cases with comparatively high sediment transport rates, which, however, becomes much less distinguishable (but still extant) at the lowest sediment concentration, although the formation of the pool–riffle is still evident. Therefore, competency in flow reversal (in bed shear stress in this specific case) may not be so evident over a pool–riffle morphology. There seems to be some quantitative discrepancy between the bed shear stress profiles from the 1D dynamic equilibrium model (Figure 11b) and the earlier 2D computational model (Figure 10b). A close examination shows that this discrepancy can be ascribed to the difference in bed elevation profiles (Figures 8 and 11a) and also the side-wall resistance (via the no-slip velocity condition) included in the 2D model.

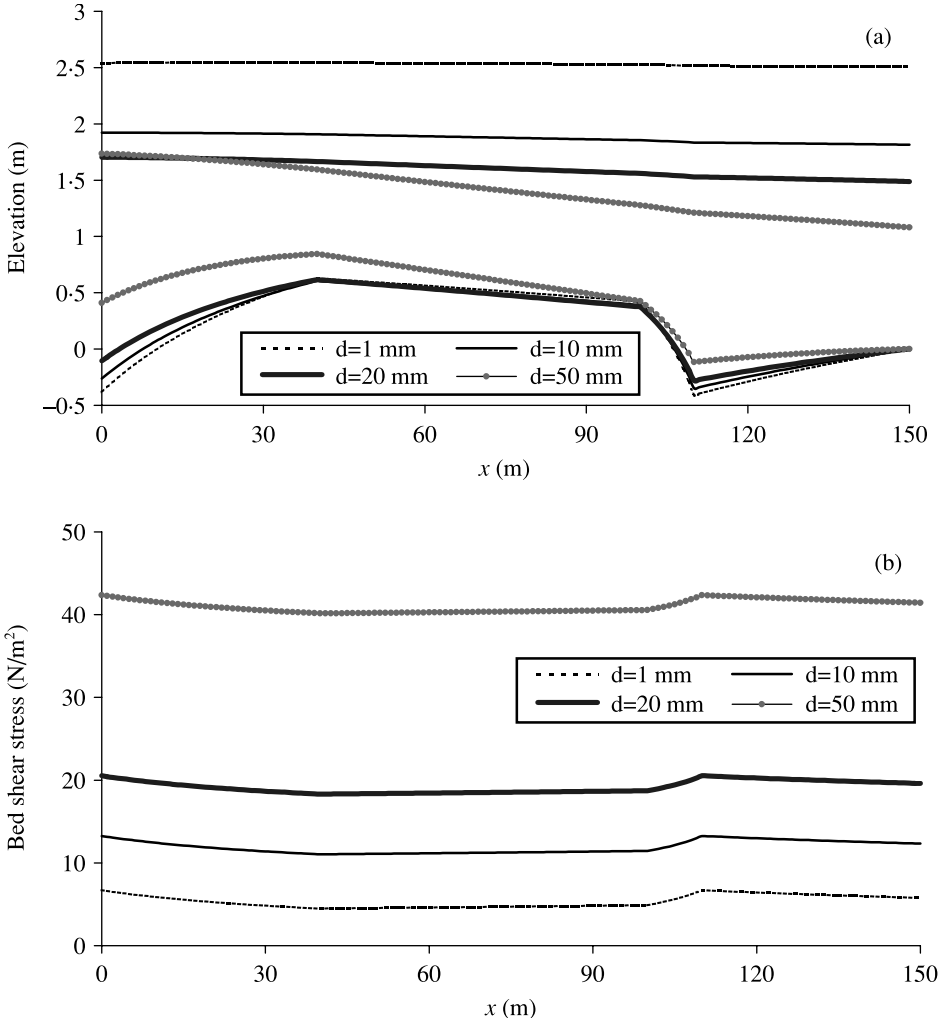

Figure 12. Pool–riffle sequences in relation to distinct sediment particle sizes: (a) bed and free surface profiles; (b) bed shear stress profiles

Illustrated in Figure 12 are the bed and free surface elevations, as well as the bed shear stress, in accord with a series of modelling exercises with constant $Q = 16$ m^3 s^{-1}, $Q_s = 0{\cdot}0016$ m^3 s^{-1} (i.e. $C = 0{\cdot}001$), $n = 0{\cdot}04$, but distinct sediment particle diameters. Apparently, the free surface profile varies considerably with sediment size, as do the flow depth and bed profile (Figure 12a). In particular, the coarser the sediment particles, the greater the height of the pool–riffle sequence, the steeper the free surface profile, and the more shallow the flow will be. This feature points to the competence of shallow and coarse sediment-laden flow in fuelling the pool–riffle morphology, in contrast to deep and fine sediment-laden flow, which is why the majority of pool–riffle sequences are seen in upland steep streams over coarse cobble beds. Interestingly, flow reversal always occurs under a fixed discharge, sediment transport rate and roughness, irrespective of sediment particle diameter (Figure 12b). Comprehending Figures 11 and 12, sediment particle size and concentration are pivotal factors dictating the formation of a pool–riffle morphology, whilst the competence of reversal is subject to specific flow and sediment characteristics.

CONCLUSIONS

A computational study is carried out on the hydraulics of a natural pool–riffle sequence in the River Lune, northern England, by deploying a depth-averaged 2D model calibrated with field observation data. The flow is

characterized by the shallow depth compared with bed material size over the riffle, which necessitates the use of distributed roughness at low discharge, and is also dictated by the constriction in channel width at the pool head. The occurrence and features of the double peak zones of bed shear velocity, velocity and Froude number are demonstrated in response to differing discharges. In particular, in line with the maximum energy slope, the primary peak zone appears at the riffle tail at low discharge and migrates upstream with increasing discharges, showing evident equalization to its surrounding hydraulic profiles. Concurrently, owing to channel constriction, the secondary peak zone remains at the pool head irrespective of discharge, but its value increases with discharge and can be as competent as that over the riffle, which indicates flow reversal.

A 1D dynamic equilibrium model is presented, which qualitatively reconstructs the pool–riffle morphology. A series of modelling exercises reveals that shallow flows heavily concentrated with coarse sediments can fuel a pool–riffle morphology more easily than deep flows with low concentrations of fine sediments. Also, under the dynamic equilibrium condition, the competence of reversal is heavily dependent upon sediment concentration.

In conclusion, channel constriction at the pool head can, but may not necessarily, lead to competent flow reversal, depending on channel geometry, flow intensity and sediment properties. The more the channel contracts, the higher the discharge and sediment concentration under dynamic equilibrium conditions, the more competent the reversal will be.

ACKNOWLEDGEMENTS

This study is supported by the Engineering and Physical Science Research Council, UK, under GR/L94987/01, and the Natural Science Foundation of China, under grant no. 59890200-3. The constructive comments of the anonymous reviewers are gratefully acknowledged.

REFERENCES

Barros AP, Colello JD. 2001. Surface roughness for shallow overland flow on crushed stone surfaces. *Journal of Hydraulic Engineering, ASCE* **127**(1): 38–52.

Booker DJ, Sear DA, Payne AJ. 2001. Modelling three-dimensional flow structures and patterns of boundary shear stress in a natural pool–riffle sequence. *Earth Surface Processes and Landforms* **26**: 553–576.

Cao Z, Carling PA. 2002a. Mathematical modeling of alluvial rivers: reality and myth. Part I: general overview. *Water and Maritime Engineering*, ICE: **154**(3): 207–219.

Cao Z, Carling PA. 2002b. Mathematical modeling of alluvial rivers: reality and myth. Part II: special issues. *Water and Maritime Engineering*, ICE: **154**(4): 297–307.

Carling PA. 1991. An appraisal of the velocity reversal hypothesis for stable pool–riffle sequences in the River Severn, England. *Earth Surface Processes and Landforms* **16**: 19–31.

Carling PA, Wood N. 1994. Simulation of flow over pool–riffle topography: a consideration of the velocity reversal hypothesis. *Earth Surface Processes and Landforms* **19**: 319–332.

Keller EA. 1971. Areal sorting of bed-load material: the hypothesis of velocity reversal. *Geological Society of America Bulletin* **82**: 753–756.

Keller EA, Florsheim JL. 1993. Velocity reversal hypothesis: a model approach. *Earth Surface Processes and Landforms* **18**: 733–740.

Lim SY. 1993. Clear water scour in long contractions. *Water Maritime and Energy,* ICE: **101**(2): 93–98.

Lim SY, Cheng NS. 1998. Scouring in long contractions. *Journal of Irrigation and Drainage Engineering, ASCE* **124**(5): 258–261.

Lisle TE. 1979. A sorting mechanism for a riffle–pool sequence: summary. *Geological Society of America Bulletin* **90**: 616–617.

Miller AJ. 1994. Debris-fan constrictions and flood hydraulics in river canyons: some implications from two-dimensional modelling. *Earth Surface Processes and Landforms* **19**: 681–697.

Nezu I, Nakagawa H. 1993. *Turbulence in Open-Channel Flows*. IAHR Monograph. IAHR: Rotterdam.

Oakey R. 2002. *The use of tracers to determine coarse-bedload transport in a gravel-bed river*. PhD dissertation, Lancaster University.

Richards KS. 1978. Simulation of flow geometry in riffle–pool sequences. *Earth Surface Processes and Landforms* **3**: 345–354.

Sear DA. 1996. Sediment transport processes in pool–riffle sequences. *Earth Surface Processes and Landforms* **21**: 241–262.

Shiono K, Knight DW. 1991. Turbulent open channel flows with variable depth across the channel. *Journal of Fluid Mechanics* **376**: 221–261.

Thompson DM, Nelson JM, Wohl EE. 1998. Interactions between pool geometry and hydraulics. *Water Resources Research* **34**: 3673–3681.

Thompson DM, Wohl EE, Jarrett RD. 1999. Velocity reversals and sediment sorting in pools and riffles controlled by channel constrictions. *Geomorphology* **27**: 229–241.

Yulistiyanto B, Zech Y, Graf WH. 1998. Free-surface flow around cylinder shallow-water modelling with diffusion-dispersion. *Journal of Hydraulic Engineering, ASCE* **124**(4): 419–429.

